3D graphical models for vascular-stent pose simulation

Leonardo Flórez-Valencia, Maciej Orkisz, Johan Montagnat

3D Graphical Models for Vascular-Stent Pose Simulation

Leonardo FLÓREZ-VALENCIA [1,2], Johan MONTAGNAT [3],
Maciej ORKISZ [1]

[1] *CREATIS, CNRS Research Unit (UMR 5515), U630 INSERM, Lyon, France,*
CREATIS, INSA, bât. B. Pascal, 7, av. J. Capelle, 69621 Villeurbanne cedex, France
maciej.orkisz@creatis.insa-lyon.fr

[2] Grupo de Ingeniería Biomédica, Departamento de Ingeniería de Sistemas y Computación,
Universidad de los Andes, Bogotá, Colombia

[3] I3S, CNRS Research Unit (UMR 6070), Nice Sophia Antipolis, France

abstract

Stents are playing an increasing role in the treatment of arterial stenoses and aneurysms. The goal of this work is to help the clinician in the pre-operative choice of the stent's length and diameter. This is done by embedding a model of the stent within a real vascular 3D image. Two models are used. First, a simple geometrical model, composed of a set of circles or polygons stacked along the vessel's centerline, is used to simulate the introduction and the deployment of the stent. Second, a simplex-mesh model with an adapted cylindrical constraint is used to represent the stent surface. Another axially constrained simplex-mesh deformable model is used to reconstruct the 3D vessel wall. We simulate the interaction between the vessel wall and the stent by imposing that the model of the vessel locally fit the shape of the deployed-stent model. Preliminary quantitative results of the vessel reconstruction accuracy are given.

keywords: vascular pathology, stenosis, stent, 3D image, simulation, simplex mesh, deformable model

1. Introduction

Stenoses and aneurysms can be seen as pathological deformations of the arterial lumen. These deformations are usually due to atherosclerosis, a disease of the arterial wall. An aneurysm is a local distension of the artery (Fig. 1 left). Its rupture can lead to hemorrhage and stroke. A stenosis is a local stricture of the arterial lumen (Fig. 1 right), due to the atherosclerotic plaque. It can lead to hypoperfusion, ischemia and infarct of organs that the artery irrigates. These diseases belong to main causes of death in western countries. An increasing number of patients with these pathologies undergo an implantation of an endovascular prosthesis or of a stent.

The stents are tubular grids that are deployed within the stenotic regions in order to push the vascular wall outwards and thus keep open a passageway for the blood flow. The endo-prostheses are similar to the stents, but covered with a blood-proof tissue. Implanted within an aneurysm, an endo-prosthesis canalizes the blood flow and
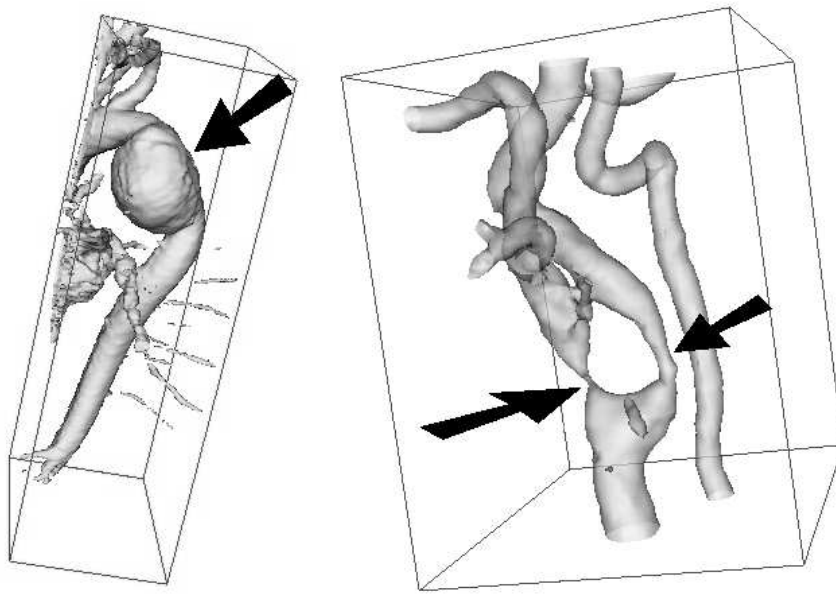
Fig. 1. Shaded-surface display of contrast-enhanced MRA images: aorta arch with an aneurysm (left), carotid artery with severe stenoses (right). Pathologies are indicated by arrows.

reduces the pressure on the arterial wall, thus preventing rupture. When folded, the stents and the endo-prostheses are slim and can be inserted into the artery, using a catheter. Deployed by shape-memory effect or by an inflating balloon, they become shorter and should fit to the diameter of the artery's healthy part. An appropriate pre-operative choice of the stent (endo-prosthesis) dimensions is necessary to avoid loosening, formation of a thrombus, embolism and obstruction of branching vessels.

The goal of our work is to aid this choice by providing a simulation tool able to represent stent-deployment within the given patient's artery. For the sake of conciseness, "stent" will be used in the sequel to denote both stents and endo-prostheses.

Several recent studies aim at extracting patients' individual vascular 3D geometry and/or at simulating radiological vascular interventions. Virtual Vascular Project [5, 15] concentrates on the simulation of insertion of surgical needles and of catheters. In MedIS-VR project virtual endoscopic viewing is used for preoperative aortic stent planning. The vessel centerline is first automatically extracted. A virtual stent is then placed along this path. Its length and its diameters are finally interactively adjusted [9]. Another project, named Geodesic, brings together automatic and semi-automatic segmentation tools and combines them with mesh generation tools in order to build patient-specific vascular
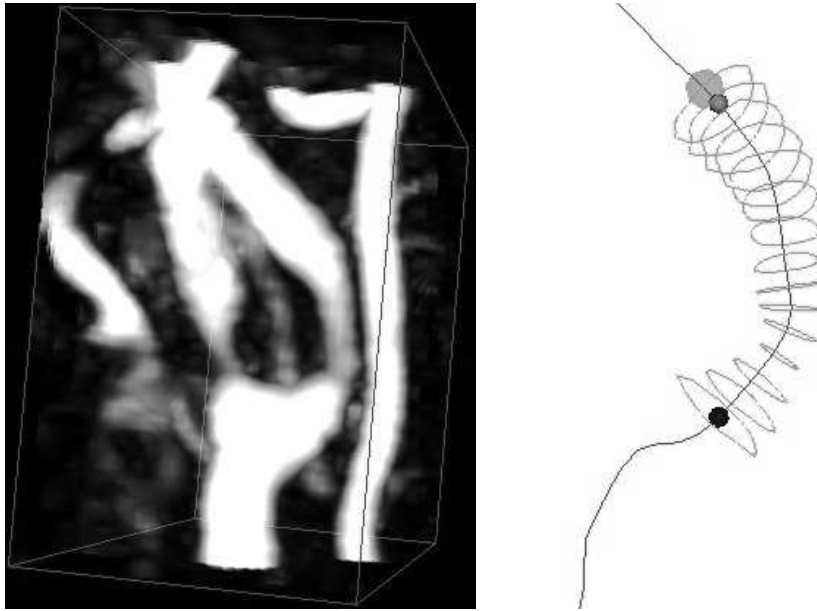
Fig. 2. Maximum intensity projection (left) of the stenosed carotid arteries from Fig. 1. Stenosed region of the internal carotid artery segmented by Maracas software: vessel centerline and stacking of contours orthogonal to this line (right).

models [19]. These models are then used for a surgical planning, *e.g.* simulation of revascularization, flow simulation, etc. This project is a recent version of an earlier work named ASPIRE [10, 11]. In [16], the patient-specific vascular geometry is automatically segmented using a tubular deformable mesh model [20]. The stent model is also a cylindrical mesh. Merging both meshes simulates artery stenting.

In our work, we follow a similar approach. However, instead of mesh merging, we attempt to simulate stent/vascular-wall interaction. The vascular lumen 3D image is first acquired using contrast-enhanced magnetic resonance angiography (MRA) technique [2]. This image is then segmented (Fig. 2) using Maracas, a software developped in our laboratory [22]. The segmentation method is based on generalized-cylinder model and provides the axial shape of the vessel, planar contours orthogonal to the vessel centerline and estimated values of local vascular lumen radii [13]. The simulation of stent insertion and deployment is carried out using a simplified geometrical model "pulled on" the centerline. This model is described in section 2. A more realistic representation of the stent and of the vessel wall surface, as well as the interaction between them, is then realized using a simplex-mesh deformable model presented in section 3.
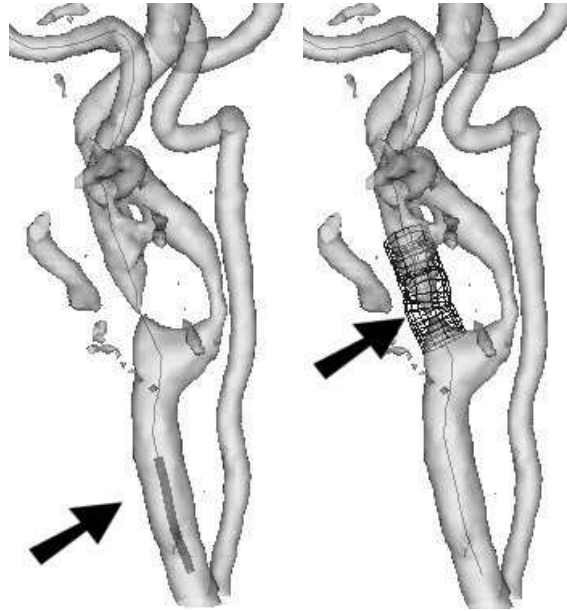
Fig. 3. Simulation of stent insertion and deployment using a simplified geometrical model: a contracted stent (left) is placed along a catheter and guided until the delivery location, once expanded (right) the stent becomes shorter. The locations of the stent are indicated by arrows.

2. Geometrical model

A generalized cylinder, as used in Maracas for vessels representation, *i.e.* a stacking of contours orthogonal to the centerline, can also be used to model stents. Let $A_p(l_p)$ and $A_v(l_v)$ be parametric 3D curves representing the centerlines of the stent and of the vessel respectively, with $l_p \in [0, 1]$ and $l_v \in [0, 1]$ the arc-length parameters. The discretized version of each centerline $A(l)$ is a set of vertices $\{\mathbf{a}_i\}$. The discretization of $A_v(l_v)$ is not uniform, while $A_p(l_p)$ has to be uniformly discretized. The absolute length of the vascular segment L_v provided by Maracas is greater than the maximum length L_{pM} of the stent. Let furthermore $C_p(l_p)$ be a planar contour orthogonal to $A_p(l_p)$ and centered at the centerline point corresponding to the arc-length l_p.

The initial model of the stent is constructed by placing predefined-shape contours $C_p(l_p)$, circular or polygonal, equally spaced along a straight axis. It is assumed that the stent does not modify the vessel's axial shape. This implicitly means that the stent is much more flexible than the vessel wall. Fitting the stent to the vessel axial shape can then be seen as a process of sweeping the predefined shape $C_p(l_p)$ along the centerline
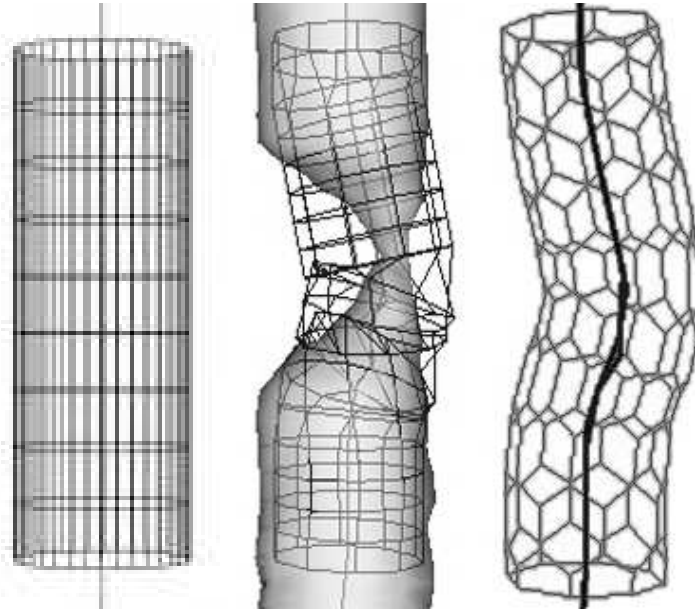
Fig. 4. Stent representation in a straight (left) and curved-centerline region: the geometrical model
generates an irregular folded surface due to intersections of contours (middle), a simplex-mesh
model generates a regular surface (right).

$A_v(l_v)$, while keeping the contour plane orthogonal to this line (Fig. 3). This is a simplified discrete process comparable to surface construction using implicit functions [1]. The axis $A_p(l_p)$ of the initial straight model of the stent is first mapped onto the vessel centerline $A_v(l_v)$. The stent model is then placed between l_{v0} and l_{vM}, where l_{v0} is a user-defined delivery point, and l_{vM} is an end point automatically deduced (for a given radius) from the length/radius relation that characterizes the stent-expansion process [12]. The radius used for this calculation can be set in two ways. The user can set its value, thus simulating a deployment based on balloon inflation. The radius can also be deduced from the vessel size estimated by Maracas at l_{v0}, thus simulating the behavior of an autoexpandable stent.

This geometrical model is very useful to simulate the displacement of the stent along the vessel centerline and to interact with the user in order to choose the delivery region and the stent parameters. Once deployed, this model provides the exact length and location of the stent. However, the surface thus constructed is not regular. The contours orthogonal to the centerline may intersect each other, where the centerline is curved (Fig. 4 middle). The surface is difficult to represent and appears locally folded. Further-

more, this model is not well-suited for the simulation of stent/vessel-wall interaction. Another model, based on a simplex mesh, is therefore used to simulate this interaction and to display the final result. This model is constrained by the centerline segment $A_v(l_v)$, $l_v \in [l_{v0}, l_{vM}]$.

3. Simplex model

Simplex meshes are discrete representations of surfaces suited to deformation [8]. In 2-simplex meshes used to represent surfaces, each vertex has exactly three neighbors. 2-simplex meshes are topologically dual to triangulations, thus making conversions back and forth easy.

In this work, we propose a specific constraint of the simplex meshes deformation framework [7] adapted to cylindrical shape deformation [4].

3.1. Model deformation

A simplex surface is a discrete model represented by a set of vertices $\{\mathbf{x}_i\}$. For deformation purposes, each vertex undergoes a displacement $\mathbf{d}_i$ controlled by an internal (regularizing) energy term and an external (data-driven) term. Unlike deformable models described by continuous equations involving physics-like elasticity and stiffness parameters (see [3] for a survey) the deformation process is not designed to mimic any physical behavior. Nevertheless, the expected properties of the surface are very similar to the continuity and smoothness constraints of these models. Internal forces involved in the deformation of a simplex surface have two components: tangential and normal. The tangential component tends to distribute the vertices so that the distances between them be uniform, while the normal component uniformizes the curvature (see [7, 8] for details). A discrete energy minimization framework leads to evolutive equation [17]:

$$\mathbf{x}_i^{t+1} = \mathbf{x}_i^t + \gamma(\mathbf{x}_i^t - \mathbf{x}_i^{t-1}) + \mathbf{d}_i^{\text{int}} + \beta\mathbf{d}_i^{\text{ext}} \tag{1}$$

where $\mathbf{x}_i^t$ denotes the location of vertex $\mathbf{x}_i$ at iteration t (with initial condition $\mathbf{x}_i^{-1} = \mathbf{x}_i^0$), $\mathbf{d}_i^{\text{int}}$ and $\mathbf{d}_i^{\text{ext}}$ are displacement components respectively owing to the internal and external forces, $\beta \in [0, 1]$ is the external force weight, and γ is a damping parameter. The latter plays the same role as viscosity in physically-based models. When γ is close to 0, the surface evolves very slowly. Conversely, when γ is close to 1 oscillations may occur. Experimentation confirms existing theoretical results according to which the fastest convergence is obtained with $\gamma \approx 0.35$. Let us note however that full theoretical demonstration of the convergence of this dicrete scheme does not exist.

The external force ensures attraction of the model towards the vessel boundary in the image. The location of the vascular-lumen boundary depends on image acquisition modality. Hence, this force is also modality-dependent and uses either gradient intensity or an iso-value dependent on the maximum intraluminal signal. Indeed, it has been

demonstrated that the actual location of the vessel boundary depends on the imaging modality and does not necessarily correspond to the gradient maximum [6]. An empirical study [21] on contrast-enhanced MRA images of vessel-phantoms with stenoses has shown that the boundary is located at 45% of the local intra-luminal maximum of the intensity. This iso-value is therefore used for the computation of the external forces. External forces are computed as displacement vectors along the direction normal to the simplex-surface. The weight of the external force (β), is to be set experimentally. In high quality data β may be close to one. In noisy data, where confidence in boundary detection is low, β should be low, too, so that the internal forces play their regularizing role. In our experimentation we used $\beta = 0.1$.
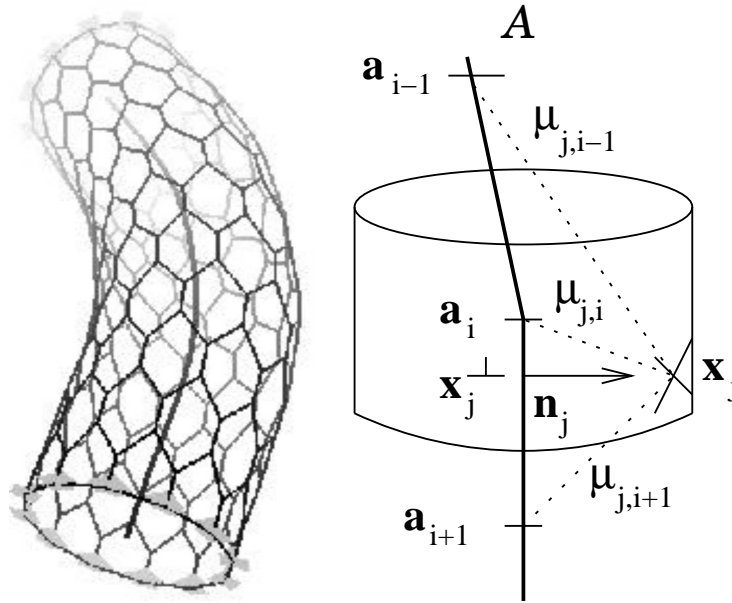

Fig. 5. Deformed cylinder (left) and notations diagram (right)

3.2. Model extension to generalized cylinders

Equation (1) defines the local displacement of each surface vertex but it does not take into account the particular shape and expected properties of the modeled object. When dealing with vessels, one expects cylindrical structures with high bending capability, for which deformations should preserve the generalized cylinder shape (Fig. 4 right and Fig. 5 left). Biomechanical models [18] are suited for that kind of physical deformations

but they are very costly. Instead, we propose an extension of our surface model.
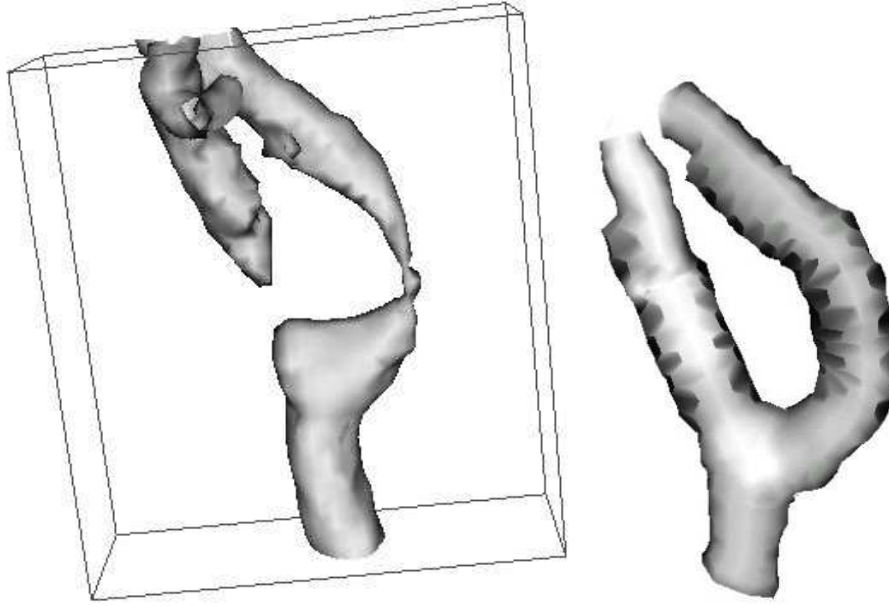

Fig. 6. Simulation of stent/vessel-wall interaction in real stenosed carotid arteries from (Fig. 1). Shaded-surface display of the region of interest in the original data (left): due to the local lack of signal in the MRA image, the more severe stenosis appears as a discontinuity of the vessel lumen. Simulated appearance of the lumen surface of the vessels of interest after insertion of virtual stents in both internal and external carotid arteries (right).

The surface is bound to the centerline: each surface vertex $\mathbf{x}_j$ is associated with three closest centerline vertices $\{\mathbf{a}_{i-1}, \mathbf{a}_i, \mathbf{a}_{i+1}\}$ (Fig. 5 right), except vertices at both ends of the cylinder surface, which are bound to two centerline vertices. Conversely, we denote $\mathcal{E}_i$ the set of surface vertices bound to the centerline vertex $\mathbf{a}_i$. Each pair of vertices $(\mathbf{a}_i, \mathbf{x}_j)$ is weighted by a coefficient μ_{ij} such that $\sum_j \mu_{ij} = 1$. These coefficients are computed automatically, based on the inverse of the distance between the vertices. When the model surface undergoes some deformation, the centerline bends accordingly through an external force resulting from the surface forces. The resulting displacement is:

$$\mathbf{d}^{\text{ext}}(\mathbf{a}_i) = \sum_{\mathbf{x_j} \in \mathcal{E}_i} \mu_{ij} \mathbf{d}^{\text{ext}}(\mathbf{x}_j) \tag{2}$$

The centerline is considered as a 1-simplex mesh in $I\!\!R^3$ and the equation (2) is used to compute its deformation owing to the external force. Conversely, the centerline bending is reported onto the surface as the sum of an axial component (each vertex tends to

follow the global motion of the axis) and a radial component (each vertex tends to align on a circle around the centerline) with:

$$
\begin{aligned}
\mathbf{d}^{\mathrm{axial}}(\mathbf{x}_j) &= \sum_{k=i-1}^{k=i+1} \mu_{kj} \mathbf{d}^{\mathrm{ext}}(\mathbf{a}_k) \\
\mathbf{d}^{\mathrm{radial}}(\mathbf{x}_j) &= \sum_{k=i-1}^{k=i+1} \mathbf{x}_j^{\perp} + \left((1-\xi) \|\mathbf{x}_j^{\perp} \mathbf{x}_j\| + \xi r_k \right) \mathbf{n}_j - \mathbf{x}_j
\end{aligned}
\tag{3}
$$

where $\mathbf{x}_j^{\perp}$ is the orthogonal projection of $\mathbf{x}_j$ onto the centerline, $\mathbf{n}_j$ (Fig. 5 right) is the unit normal vector of the centerline in $\mathbf{x}_j^{\perp}$ (*i.e.* $\mathbf{n}_j = \mathbf{x}_j^{\perp}\mathbf{x}_j / \|\mathbf{x}_j^{\perp}\mathbf{x}_j\|$), r_k is the radius (mean distance of the surface vertices to the centerline) in $\mathbf{a}_k$ and ξ is a radial weight. In our experimentation this parameter varied between 0.3 and 0.8. With small values of ξ circularity constraint is weak and complex cross-sectional shapes can be recovered. Larger values are used when data are not reliable. When ξ tends to one, the cross-sections tend to be circular with constant radius along the cylinder.

The surface vertices are thus submitted to the internal and external forces (local forces) plus the axial and radial forces (cylindrical forces). Let $\lambda \in [0,1]$ weight the contributions of the local and cylindrical forces. The equation (1) becomes:

$$
\mathbf{x}_i^{t+1} = \mathbf{x}_i^t + \gamma(\mathbf{x}_i^t - \mathbf{x}_i^{t-1}) + (1-\lambda)\left(\mathbf{d}_i^{\mathrm{int}} + \beta \mathbf{d}_i^{\mathrm{ext}} \right) + \lambda \left(\mathbf{d}^{\mathrm{axial}}(\mathbf{x}_i^t) + \mathbf{d}^{\mathrm{radial}}(\mathbf{x}_i^t) \right)
\tag{4}
$$

In our application strong contribution of the cylindrical forces was desired. Hence, we experimentally set $\lambda = 0.95$.

3.3. Model initialization

Deformable models are sensitive to their initialization as they usually converge towards a local minimum of their energy functional. In our application however, Maracas accurately extracts centerline points $\{\mathbf{a}_i\}$ and roughly estimates a set of radii $\{r_i\}$. This provides an initialization of the simplex-mesh model close to the vessel boundary and, together with the axial constraint, can be successfully used for 3D segmentation of the vessel. However, the model of the vessel-lumen surface has to interact with a model of the stent in order to converge towards a realistic representation of the stented vessel.

3.4. Stent modeling

Stent-deployment simulation using the simplified geometrical model described in the section 2, provides the stent-axis mapping onto the vessel centerline calculated by Maracas, between the bounds l_{v0} and l_{vM}, for a given stent radius r. The stent surface is represented using a new cylindrical simplex model combining the mapped centerline and the radius r. Once constructed, this model remains static, *i.e.* it is not submitted to deformations. In the stent area (between l_{v0} and l_{vM}), the shape of the vessel-surface model is controlled by the stent shape rather than the external forces extracted from the image data. Therefore, the external force of the vessel-surface model is locally set to zero. Instead, the corresponding section of the vessel-surface model is attracted by the surface of the stent model.
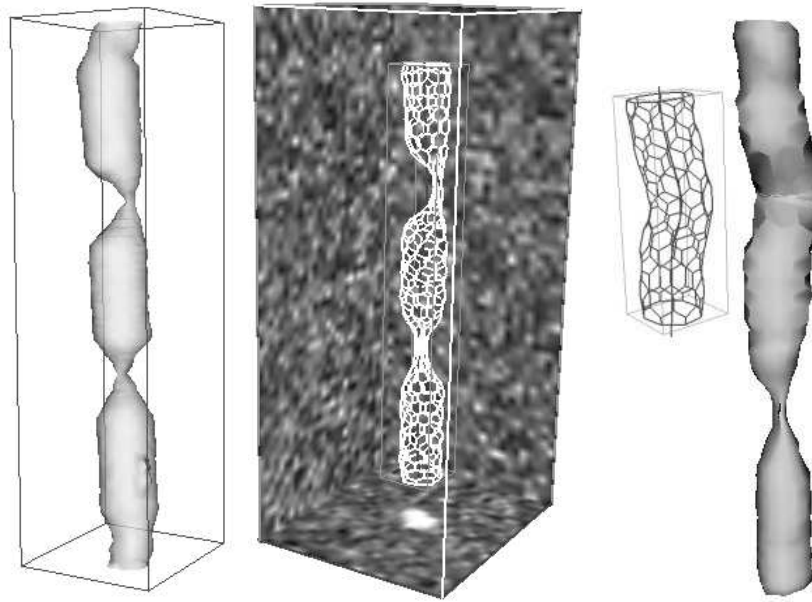
Fig. 7. Simulation of stent/vessel-wall interaction in a physical phantom of stenosed vessel. From left to right: shaded-surface display of an MRA image of the phantom, simplex mesh resulting from its segmentation and embedded in the original image, deformed stent model, and shaded-surface display of the vessel with the stent inside.

4. Results and conclusion

The above described procedure was applied to simulate stent introduction and expansion in real arteries (Fig. 6) and in six phantoms (Fig. 7). The visualisation of a virtual stent deployed in real MRA data volume is useful for preoperative assessment of the stent's diameter and length.

The simulation of the interaction between the vascular wall and the stent generates a realistic view of the luminal shape modification induced by the stent. The simplex-mesh deformable model used for this simulation is applicable to vascular-image segmentation and quantification (Fig. 8). Compared to the known percentages of the stenoses in the images of phantoms, the average absolute error of the quantification of the stenosis percentage was 7.3%. The largest errors occurred in complex stenoses, where the shape was no more cylindrical, and in the most severe stenoses (95% of narrowing), due to the lack of signal.

Our simulation is based on the simplifying assumption that the stent does not modify the axial geometry of the vessel. However, it has been demonstrated [14] that the
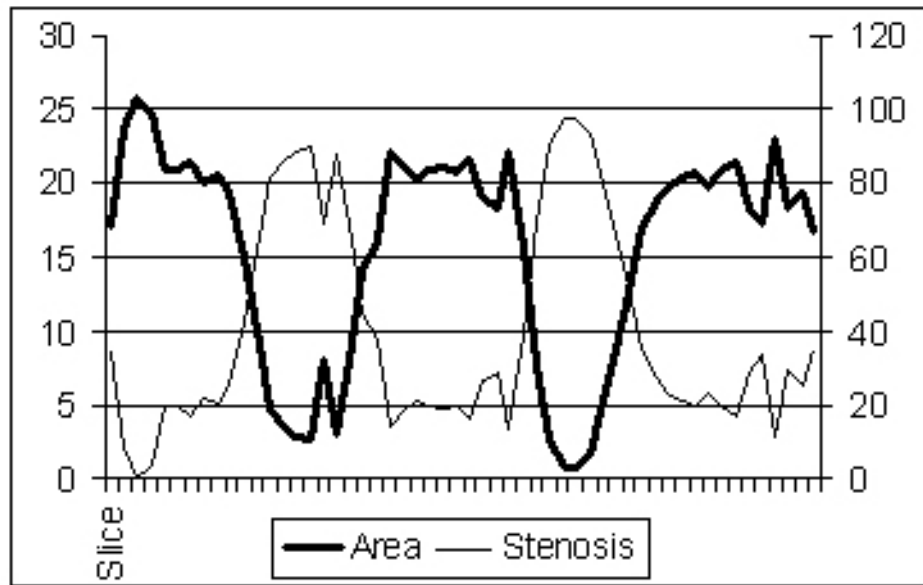
Fig. 8. Quantification curves obtained from the phantom (Fig. 7) segmented by our simplex model. The scale on the left corresponds to the units of the area (mm^2), while the scale on the right corresponds to the percentage of the local narrowing of the vessel compared to a reference cross-section.

stent may locally change the vessel's curvature. As the stent tends to locally stiffen the vessel, the latter may be stretched outside the stented section, thus modifying its actual dimensions. Axial stiffness can be included in our deformable model, in order to simulate this phenomenon. However, this improvement of the model is not straightforward. The link between the weighting coefficient of the stiffness force and the physical properties of the vessels is not obvious. Furthermore, these properties are locally modified by the presence of atherosclerotic plaque that is more or less rigid depending on its composition. Moreover, the vessels within the body are not free, their shape strongly depends on the influence of the surrounding tissues. These open questions leave a wide field for further research combining biomechanical modelling and multi-modality image processing including high-resolution MR, computed tomography and intravascular ultrasound.

5. Acknowledgements

References

1990

[1] Bloomenthal, J. and Wyvill, B. (1990). Interactive techniques for implicit modeling. *Computer Graphics*, 24(2):109–116.

1995

[2] Douek, P. C., Revel, D., Chazel, S., Falise, B., Villard, J., and Amiel, M. (1995). Fast MR angiography of the aortoiliac arteries and arteries of the lower extremity: value of bolus-enhanced, whole-volume subtraction technique. *American Journal of Radiology*, (165):431–437.

1996

[3] McInerney, T. and Terzopoulos, D. (1996). Deformable models in medical image analysis: a survey. *Medical Image Analysis*, 1(2):91–108. TORONTO-004.

1997

[4] Montagnat, J. and Delingette, H. (1997). A Hybrid Framework for Surface Registration and Deformable Models. In *Proceedings of Computer Vision and Pattern Recognition (CVPR)*, pages 1041–1046, San Juan, Puerto Rico.

1998

[5] Abdoulaev, G., Cadeddu, S., Delussu, G., Donizelli, M., Fromaggia, L., Gianchetti, A., Gobbetti, E., Leone, A., Manzi, C., Pili, P., Scheinine, A., Tuveri, M., Varone, A., Veneziani, A., Zanetti, G., and Zorcolo, A. (1998). ViVa: The Virtual Vascular project. *IEEE Transactions on Information Technology in Biomedicine*, 22(4).

[6] Hoogeveen, R., Bakker, C., and Viergever, M. (1998). Limits to the accuracy of vessel diameter measurement in MR Angiography. *Journal on Magnetic Resonance Imaging*, 8(6):1228–1235.

[7] Montagnat, J. and Delingette, H. (1998). Globally constrained deformable models for 3D object reconstruction. *Signal Processing*, 71(2):173–186.

1999

[8] Delingette, H. (1999). General Object Reconstruction based on Simplex Meshes. *International Journal of Computer Vision*, 32(2):111–146.

[9] Stern, C., Wildermuth, S., Weissmann, J., Stucki, P., Hilfiker, P., and Debatin, J. F. (1999). Predictive medicine: Computational techniques in therapeutic decision-making. In *Computer Assisted Radiology and Surgery (CARS)*, pages 176–180, Paris, France.

[10] Taylor, C., Draney, M., Ku, J., Parker, D., Steele, B., Wang, K., and Zarins, C. (1999). Predictive medicine: Computational techniques in therapeutic decision-making. *Computer Aided Surgery*, (4):231–247.

[11] Wang, K., Dutton, R., and Taylor, C. (1999). Improving geometric model construction for blood flow modeling. *IEEE Engineering in Medicine and Biology*, 18(6):33–39.

2000

[12] Dumoulin, C. and Cochelin, B. (2000). Mechanical behaviour modelling of balloon-expandable stents. *Journal of Biomechanics*, 33:1461–1470.

[13] Hernández-Hoyos, M., Anwander, A., Orkisz, M., Roux, J. P., Douek, P. C., and Magnin, I. E. (2000). A Deformable Vessel Model with Single Point Initialization for Segmentation, Quantification and Visualization of Blood Vessels in 3D MRA. In *Medical Image Computer and Computer Assisted Intervention (MICCAI)*, pages 735–745, Pittsburgh, PA, USA.

[14] Wentzel, J., Whelan, D., Van Der Giessen, W., Van Beusekom, H., Andhyiswara, I., Serruys, P., Slager, C., and Krams, R. (2000). Coronary stent implantation changes 3D vessel geometry and 3D shear stress distribution. *Journal of Biomechanics*, 33:1287–1295.

[15] Zorcolo, A., Gobbetti, E., Zanetti, G., and Tuveri, M. (2000). A Volumetric Virtual Environment for Catheter Insertion Simulation. In *Eurograhics Workshop on Virtual Enviroments (EGVE)*, Amsterdam, The Netherlands.

2001

[16] Cebral, J. R., Lohner, R., Soto, O., Choyke, P. L., and Yim, P. J. (2001). Patient-Specific Simulation of Carotid Artery Stenting Using Computational Fluid Dynamics. In *Medical Image Computer and Computer Assisted Intervention (MICCAI)*, pages 153–160, Utrecht, The Netherlands.

[17] Montagnat, J., Delingette, H., and Ayache, N. (2001). A review of deformable surfaces: topology, geometry and deformation. *Image and Vision Computing*, 19(14):1023–1040.

[18] Pham, Q. C., Vincent, F., Clarysse, P., Croisille, P., and Magnin, I. E. (2001). A FEM-based deformable model for the 3D segmentation and tracking of the heart in cardiac MRI. In *International Symposium on Image and Signal Processing and Analysis*, pages 250–254, Pula, Croatia.

[19] Wilson, N., Wang, K., Dutton, R. W., and Taylor, C. (2001). A Software Framework for Creating Patient Specific Geometric Models from Medical Imaging Data for Simulation Based Medical Planning of Vascular Surgery. In *Medical Image Computer and Computer Assisted Intervention (MICCAI)*, pages 449–456, Utrecht, The Netherlands.

[20] Yim, P. J., Cebral, J. R., Mullick, R., Marcos, H. B., and Choyke, P. L. (2001). Vessel Surface Reconstruction With a Tubular Deformable Model. *IEEE Transactions on Medical Imaging*, 20(10):1411–1421.

2002

[21] Hernández-Hoyos, M. (2002). *Segmentation anisotrope 3D pour la quantification en imagerie vasculaire par résonance magnétique*. PhD thesis, INSA de Lyon, France.

[22] Hernández-Hoyos, M., Orkisz, M., Puech, P., Mansard, C., Douek, P. C., and Magnin, I. E. (2002). Computer-assisted analysis of three-dimensional angiograms. *RadioGraphics*, 22:421–436.